JVI Journals.ASM.org

Molecular Characterization of Feline Infectious Peritonitis Virus Strain DF-2 and Studies of the Role of ORF3abc in Viral Cell Tropism

Ádám Bálint,[a,e] Attila Farsang,[b,e] Zoltán Zádori,[c,e] Ákos Hornyák,[a,e] László Dencső,[a] Fernando Almazán,[d] Luis Enjuanes,[d] and Sándor Belák[e,f]

Department of Virology, Agricultural Office Veterinary Diagnostic Directorate, Budapest, Hungary[a]; Agricultural Office Directorate of Veterinary Medicinal Products, Budapest, Hungary[b]; Institute for Veterinary Medical Research, Centre for Agricultural Research, Hungarian Academy of Sciences, Budapest, Hungary[c]; Department of Molecular and Cell Biology, Centro Nacional de Biotecnología (CNB-CSIC), Campus Universidad Autónoma de Madrid, Madrid, Spain[d]; Department of Biomedical Sciences and Veterinary Public Health, Swedish University of Agricultural Sciences, Uppsala, Sweden[e]; and Department of Virology, Immunobiology and Parasitology, National Veterinary Institute, Uppsala, Sweden[f]

The full-length genome of the highly lethal feline infectious peritonitis virus (FIPV) strain DF-2 was sequenced and cloned into a bacterial artificial chromosome (BAC) to study the role of ORF3abc in the FIPV-feline enteric coronavirus (FECV) transition. The reverse genetic system allowed the replacement of the truncated ORF3abc of the original FIPV DF-2 genome with the intact ORF3abc of the canine coronavirus (CCoV) reference strain Elmo/02. The *in vitro* replication kinetics of these two viruses was studied in CrFK and FCWF-4 cell lines, as well as in feline peripheral blood monocytes. Both viruses showed similar replication kinetics in established cell lines. However, the strain with a full-length ORF3 showed markedly lower replication of more than 2 $\log_{10}$ titers in feline peripheral blood monocytes. Our results suggest that the truncated ORF3abc plays an important role in the efficient macrophage/monocyte tropism of type II FIPV.

Feline coronaviruses (FCoVs) are important pathogens of domestic cat populations worldwide. FCoVs are also widespread among wild *Felidae*, including African and Mountain lions (7, 26). It is also a considerable risk factor for captive and free-ranging cheetahs (22).

FCoVs have two serotypes (12, 24, 27, 30), and both occur in two pathotypes: the avirulent feline enteric coronavirus (FECV) and the virulent feline infectious peritonitis virus (FIPV) (36). The marked difference between the two pathotypes is that the primary replication site of FECV is localized in the lower portion of the intestinal tract, whereas FIPV efficiently replicates in macrophages and monocytes and can cause generalized disease (1, 2, 13, 21, 36). FIPVs arise most probably from FECV in the infected cat by genetic alterations (49) affecting the spike (S) gene (41), ORF3abc (9, 10, 37, 49), and ORF7ab (29, 49). Most authors suspect a role for the ORF3abc region in the development of FIP. FECVs have three open reading frames (ORFs) in this region (21), and the protein sequences coded by these ORFs in different isolates are invariably uniform in length and sequence. In contrast, the majority of FIPVs contain at least one deletion in the ORF3abc region regardless of their serotype. Most of the deletions occur in ORF3c, but they are not rare in ORF3a and ORF3b (9, 49). Nondeleted ORF3c of FIPVs accumulates four times more unique nonsynonymous amino acid mutations in the 3′ regions than the FECVs (38). These data suggest that functional gene products of ORF3abc are the prerequisites for the replication of the avirulent pathotype in the enteric tract, but genetic alterations in this region may enhance the fitness of the virus replicating in macrophage cells (9).

To study the role of ORF3abc in the development of the macrophage/monocyte tropism of the FCoVs, we cloned a cDNA copy of the full-length genome of FIPV DF-2 into a bacterial artificial chromosome (BAC). The full-length infectious clone of FIPV DF-2 allowed us to replace the originally truncated ORF3abc of DF-2 with an intact, genetically closed orthologous ORF3abc obtained from canine coronavirus (CCoV) Elmo/02 (39) and rescue recombinant viruses. The *in vitro* growth properties of the virus pair, differing only in their ORF3abc, were determined in cell lines and feline blood monocytes. While both viruses showed relatively similar replication kinetics in CrFK and FCWF-4 cell lines, the ORF3-complemented strain showed markedly lower replication (more than 2 $\log_{10}$ titers) in feline peripheral blood monocytes. These results suggest that the truncated ORF3abc plays an important role in the efficient macrophage/monocyte tropism of type II FIPV.

MATERIALS AND METHODS

Cells and viruses. *Felis catus* whole fetus 4 (FCWF-4) and Crandell-Rees feline kidney (CrFK) cell lines and feline blood monocytes were used for virus propagation and titration. The cell lines were maintained as monolayer cultures in Dulbecco's modified Eagle medium (Sigma-Aldrich, St. Louis, MO) supplemented with 10% fetal bovine serum (FBS), 0.2 mM glutamine, 100 U/ml penicillin, 0.1 mg/ml streptomycin, 0.25 μg/ml amphotericin B, 1 mM sodium pyruvate, and 1% nonessential amino acids (Sigma-Aldrich). Feline blood monocytes originating from five specific-pathogen-free (SPF) cats were isolated as described earlier (14). Briefly, blood mononuclear cells from 5 ml anticoagulated blood were purified on Histopaque-1077 (Sigma-Aldrich) according to the manufacturer's recommendations. The cells were seeded in a 24-well dish at a density of 2×10^6 cells/ml and cultivated at 37°C with 5% CO_2. Cells were washed twice with RPMI 1640 at 2 and 24 h after seeding to remove nonadherent cells.

For the determination of the growth kinetics of the viruses in the two cell lines, cells were infected at multiplicity of infection (MOI) of 0.1. After

Received 3 February 2012 **Accepted** 12 March 2012
Published ahead of print 21 March 2012
Address correspondence to Ádám Bálint, balintad@oai.hu.

doi:10.1128/JVI.00189-12

TABLE 1 Primers used to generate overlapping fragments of the FIPV genome to construct full-length clone pBFIPV-DF-2

Primer code	Nucleotide sequence (5′→3′)	Nucleotide position[c] (5′)
5′DF2F[a]	*GAGCTCGTTTAGTGAACCGT*ACTTTTAAAGTAAAGTGAG	1
5′ SfiIR	CTCACTTTACTTTAAAAGTACGGTTCACTAAACGAGCTC	19
5′DF2R	GGCACAATGGTACTCCTCTCCT	763
IVF-	CTCCTTACCGAACCTTCCGTCATGT	536
IVR	GACACTGACCGTTGGTGGCGTATAA	9004
VF	GGTGTTCCTTTATGATTCCCTACCA	8677
VR	CACAGAACAGTGCAAGCATGACACC	10271
VIF	CTGTCTTATGGCTCTCTGTGTGACG	9851
VIR	CTCTGATCAATAGTGGTGCCTTGTA	12399
VIIF	ACAGGACTCTTATGGTGGCGCATCT	12166
VIIR	CACCACAGACATGTGCACCTTCAAC	17257
VIIIF	CAACATACCAGGCTACCACACATTG	17154
VIIIR	ACTCTAGGCTGATACATAGTTCTGG	24277
IIIF	CAGGCTTGACGAACTGAGTGCTGAT	23861
IIIR	TGGCAGGTAGTAGGTGTGAGTGAGC	27608
3′ DF2F	GCCGTGCTTGAAAAATTAGGTG	27264
3′ DF2R[b]	*GAGATGCCATGCCGACCC*TTTTTTTTTTTTTTTTT	29038
3′ SacIIF	AAAAAAAAAAAAAAAAAAGGGTCGGCATGGCATCTC	29056
5′ SfiIF	CCTGGTTGCTACGCCTGAATAAGTG	732
3′ SacIIR	AACAATGGAAGTCCGAGCTCATCGC	7440

[a] Bases in italics are part of the CMV promoter.
[b] Bases in italics are part of the HDV RZ sequence.
[c] Primer positions correspond to the sequence of FIPV DF-2, except for those of 5′ SfiIF and 3′ SacIIR, which correspond to the sequence of pBeloBAC 11.

1 h of adsorption at 37°C, cells were washed twice with the medium and incubated at 37°C with 5% CO_2. To determine the growth kinetics of the viruses in blood monocytes, cells were infected at an MOI of 5, and after 1 h of adsorption at 37°C, monocytes were gently washed five times with the medium to remove residual virus and incubated at 37°C with 5% CO_2.

Titers of the extracellular and intracellular viruses were determined by the titration of cell culture supernatants collected at different time points from CrFK cells. Intracellular virus titers were determined after washing monocytes five times with RPMI 1640, followed by two freeze-thaw cycles. Supernatant was collected after low-speed centrifugation (3,000 × *g* for 10 min) and added to the original culturing volume with RPMI 1640. The titers were calculated as 50% tissue culture infectious doses ($TCID_{50}$)/ml with the Reed and Muench method (40).

The FIPV DF-2 strain was kindly provided by Berndt Klingeborn (SVA, Uppsala, Sweden). The CCoV Elmo/02 strain was kindly provided by Canio Buonavoglia (University of Bari, Italy).

RNA extraction and cDNA synthesis. RNA was extracted from virus stocks using the QIAamp viral RNA minikit (Qiagen, Hilden, Germany) by following the manufacturer's instructions. To obtain long cDNA copies of the viral genome, the SuperScript III first-strand synthesis system (Invitrogen, Carlsbad, CA) and gene-specific primers were used by following the manufacturer's recommendations.

Sequence analysis. The complete genome of FIPV DF-2 (GenBank accession number JQ408981) was determined by the sequencing of overlapping PCR fragments amplified with KOD hot start DNA polymerase (Merck, Darmstadt, Germany). DNA was sequenced with the BigDye V3.1 Terminator sequencing kit (Applied Biosystems, Foster City, CA) and an automated ABI 377 DNA sequencer (Applied Biosystems). Sequence assembly and comparison were performed with the SeqMan and MegAlign programs (Lasergene, Madison, WI), respectively. The full-length pBFIPV-DF-2-R3i clone (GenBank accession number JQ408980) was sequenced with the Applied Biosystems SOLiDTM 4.0 system according to the manufacturer's recommendations. For the in-depth comparative sequence analysis, the DF-2-derived vaccine strain was used (GenBank accession no. DQ286389).

Plasmids and bacteria strains. Plasmid pBeloBAC 11 (50) was kindly provided by H. Shizuya and M. Simon (California Institute of Technology, Pasadena, CA). Maximum-efficiency DH10B competent *Escherichia coli* cells (Invitrogen) were transformed by heat shock according to the manufacturer's instructions. For large-scale DNA preparation, the BAC vector and recombinant BACs were isolated with the Qiagen large construct kit (Qiagen) according to the manufacturer's specifications.

Construction of a full-length cDNA clone of FIPV DF-2. Although FCoV type I is more predominant in the field, the FIPV type II strain was selected for cloning, since no true type I FECV strain was adapted to cell cultures (38), therefore the recovery of the recombinant FCoV type I virus with intact 3abc is of high risk. Based on the data of the full-length genomic sequence of FIPV DF-2, primers were designed to amplify overlapping fragments of the whole genome (Table 1). Long-range PCR assays were performed using KOD hot start DNA polymerase (Merck) to generate PCR products ranging from 0.7 to 8.5 kb. Clones generated from the PCR fragments were used to construct the final full-length clone of the FIPV DF-2 genome. Restriction enzyme cleavage and cloning steps were performed according to standard protocols (42). Restriction endonucleases and DNA-modifying enzymes were purchased from Fermentas (Vilnius, Lithuania) and New England BioLabs (Beverly, MA).

The full-length cDNA clone of FIPV DF-2 was constructed in several steps (Fig. 1). In the first one, the pBeloBAC11 vector was digested with SfiI and SacII, and a multiple-cloning site containing SfiI, NarI, BstBI, ClaI, BamHI, XhoI, AsiSI, AvrII, and SacII recognition sites was inserted into the vector. Two DNA fragments, one containing the poly(A) tail of the genome, the hepatitis delta virus (HDV) ribozyme, and the bovine growth hormone termination and polyadenylation sequences (BGH) and the other containing the 3′ part of the M gene, the whole N gene, ORF7ab, and 3′ untranslated region (UTR), were amplified by PCR using the primers 3′SacIIF/3′SacIIR and 3′DF2F/3′DF2R, respectively. These two fragments were joined together by PCR, digested with AvrII and SacII, and cloned into pBeloBAC11 to get pBFIPV-I. By following a similar approach, two fragments containing the cytomegalovirus (CMV) immediate-early promoter upstream of the FIPV DF-2 genome and the 5′ UTR of DF-2 fused to the 5′ portion of the ORF1a gene were amplified using the primers 5′SfiIF/5′SfiIR and 5′DF2F/5′DF2R, respectively. These two fragments were merged by joining PCR, digested with SfiI and NarI, and cloned into pBFIPV-I to obtain pBFIPV-I-II. In the next step, a fragment containing the S, ORF3abc, E, M, and partial N genes of the DF-2 genome was amplified using primers IIIF and IIIR, and it was cleaved with AsiSI

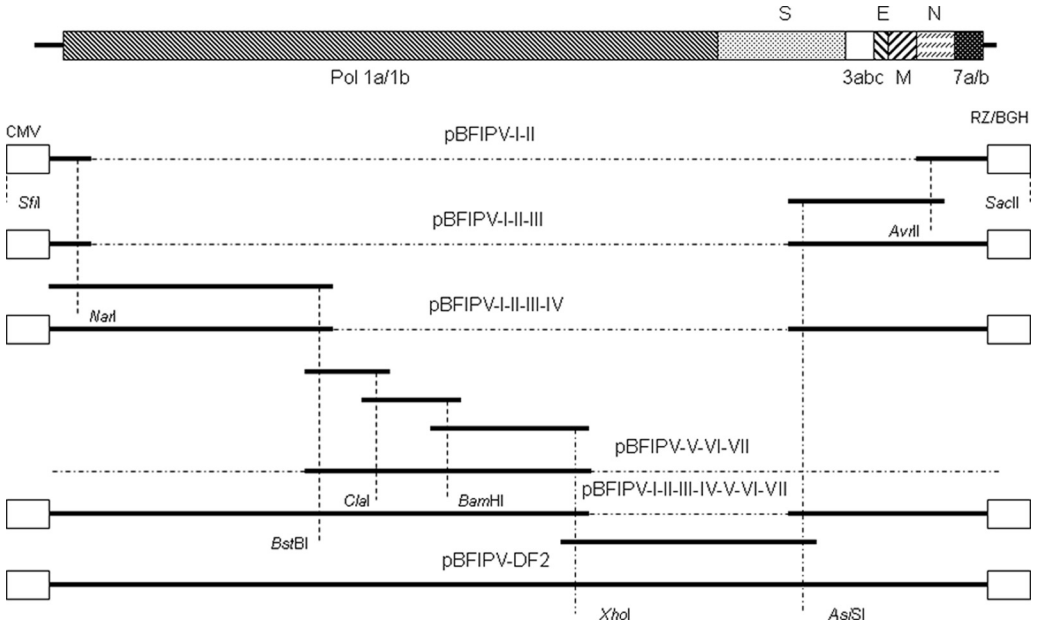

FIG 1 Cloning strategy for the FIPV DF-2 genome. Viral genes are represented by shaded boxes on the genome. Open boxes represent the 5′ and 3′ accessory sequences of the vector. Genome parts are represented with continuous boldface lines.

and AvrII and cloned into pBFIPV-I-II to obtain pBFIPV-I-II-III. Using the primers IVF and IVR, the 5′ half of ORF1ab was amplified, digested with NarI and BstBI, and cloned into pBFIPV-I-II-III to get pBFIPV-I-II-III-IV. Three fragments covering the 3′ half of ORF1ab were amplified with primers VF, VR, VIF, VIR, VIIF, and VIIR, digested with BstBI, ClaI, BamHI, and XhoI, and cloned into pBeloBAC11 to obtain pBFIPV-V-VI-VII. The two large plasmid constructs were cleaved with BstBI and XhoI and joined to get pBFIPV-I-II-III-IV-V-VI-VII. In the last step, the fragment containing the 3′ end of ORF1ab and the whole S gene was amplified using the primers VIIIF and VIIIR, digested with XhoI and AsiSI, and cloned to get the final pBFIPV-DF-2 clone. Sequences of the subclones as well as the final clone were verified by sequence analysis.

Generation of a recombinant FIPV containing intact ORF3abc. The whole ORF3 region of CCoV Elmo/02 was amplified with primers ELMO5F and ELMO3R (Table 2). A second PCR encompassing the 3′ part of the S gene was amplified with primers IIIF and ELMO5R. A third PCR using primers ELMO3F and 3′SacIIR amplified the genome downstream of the S gene and the 3′ accessory elements. The three PCRs were joined by fusion PCRs, resulting in the replacement of the truncated ORF3abc of DF-2 with the intact ORF3abc of CCoV Elmo/02. The fragment was digested with AsiSI and SacII and cloned into pBFIPV-DF-2 to obtain pBFIPV-DF-2-R3i.

Transfection and recovery of the recombinant viruses from the cDNA clones. FCWF-4 cells were grown to 70% confluence in 25-cm^2 tissue culture flasks and transfected with 10 μg of pBFIPV-DF-2 DNA using 20 μl of TurboFect *in vitro* transfection reagent (Fermentas, Vilnius, Lithuania) according to the manufacturer's specifications. The cells were incubated at 37°C for 72 h and were checked for the development of cytopathic effect (CPE).

Detection of the genomic and replicative RNA by quantitative real-time PCR. To measure the copy numbers of the genome and replicative forms of the recombinant FCoVs, two TaqMan assays targeting the 5′ end of the FIPV DF-2 genome and the N gene subgenomic (sg) mRNA were applied using the Qiagen OneStep reverse transcription-PCR (RT-PCR) kit (Qiagen) according to the manufacturer's recommendations. The reaction mix contained 1× Qiagen OneStep RT-PCR buffer, 0.4 mM deoxynucleoside triphosphates (dNTPs), 600 nM forward (DF2F) and reverse (ORF1R or NR) primers, 200 nM probe (DF2P) labeled with 5′ 6-carboxyfluorescein (FAM)/3′ black hole quencher 1 (BHQ-1) (Table 3), 20 U RiboLock RNase inhibitor (Fermentas), 1 μl Qiagen OneStep RT-PCR enzyme mix, and 5 ng template RNA in a 25-μl reaction volume. The parameters of the thermoprofile were 50°C for 30 min, 94°C for 15 min, 45 cycles of 94°C for 30s, 54°C for 30 s, and 72°C for 30 s, followed by 72°C for 7 min. Fluorescence signal data were collected for 5 s after the primer annealing with 470-nm excitation and 510-nm detection. All reactions were run in a Corbett Research Rotor-Gene real-time amplification system (RG-6000; Corbett Research, Mortlake, Australia). An RNA standard was generated with the same primers as those used for PCR with a 5′ T7 overhang of the forward primer applying the MEGAscript T7 kit (Ambion, Cambridgeshire, United Kingdom) according to the manufacturer's instructions. The regression lines between amounts of RNAs and the corresponding threshold cycle (C_T) values were calculated using Rotor-Gene software, version 6.0.19 (Corbett Research). Copy numbers of viruses propagated on FCWF-4 and CrFK cells were determined from cell

TABLE 2 Primers used to insert the intact ORF3abc region of CCoV strain ELMO/02 to construct full-length clone pBFIPV-DF-2-R3i

Primer code	Nucleotide sequence[a] (5′→3′)	Nucleotide position[b] (5′)
ELMO5F	AATTCCTTAAGAACTAAAC*AAATGAGTCAATACAGGTCT*	24825
ELMO5R	*AGACCTGTATTGACTCATTT*GTTTAGTTCTTAAGGAATT	24843
ELMO3F	TTCTGGCTCCTGTTGATAATTATATTGATA	25682
ELMO3R	TATCAATATAATTATCAACAGGAGCCAGAA	25711

[a] Bases in italics are part of ORF3a of CCoV ELMO/02.
[b] Primer positions correspond to the sequence of FIPV DF-2.

TABLE 3 Primers applied for the detection of genomic and sg RNA of the recombinant FCoVs after infection of FCWF-4 and CrFK cell lines and feline blood monocytes

Primer code	Nucleotide sequence (5′→3′)	Nucleotide position[c] (5′)
DF2F[a,b]	TAGCGTGGCTATAACTCTTCTT	22
DF2P[a]	6-FAM-GTCCGAAGACAAATCTAGCACAAGGCT-BHQ-1	81
ORF1R[a]	AAGGAAGGCTAGGAACGTTGAC	377
ORF3CR[b]	TGAGAAAAGGCTGCATTGTAAA	25571
NR[b]	CACGAGAGTTAGAACGACCACG	26754

[a] Used to detect genomic RNA.
[b] Used to detect sg RNA.
[c] Primer positions correspond to the sequence of FIPV DF-2.

lysates, while intracellular copy numbers of the recombinant viruses grown on feline blood monocytes were determined after adsorption (1 h postinfection [p.i.]) and 24 h p.i., respectively, as described above.

Detection of sg ORF3abc mRNAs by RT-PCR. RT-PCR targeting the transcription of sg mRNAs in the ORF3abc region was performed using the Qiagen OneStep RT-PCR kit (Qiagen). The reaction mix contained 1× Qiagen OneStep RT-PCR buffer, 0.4 mM dNTPs, 600 nM forward (DF2F) and reverse (ORF3CR) primers (Table 3), 20 U RiboLock RNase inhibitor (Fermentas), 1 μl Qiagen OneStep RT-PCR enzyme mix, and 5 ng template RNA in a 25-μl reaction volume. The parameters of the thermoprofile were 50°C for 30 min, 94°C for 15 min, 35 cycles of 94°C for 30 s, 58°C for 30 s, and 72°C for 2 s, and then 72°C for 7 min. PCR products were analyzed on 1% agarose gel containing 1× GelRed (Biotium, Hayward, CA).

RESULTS

Genome organization of FIPV DF-2. The FIPV DF-2 virus used in this study was isolated from the spleen of a cat that succumbed to FIP (17). The genome showed 99% nucleotide homology to FIPVWSU-79/1146 (15), except in the ORF3abc region. Similarly high homology to the only available sequence of Nor15 was found as well (23).

SimPlot analysis (31) with type I FCoV UU8 and type II CCoV strain NTU 336 revealed the presence of type II CCoV-related sequence in the FIPV DF-2 genome from nucleotide (nt) 13344 in the 5′ half of the ORF1b gene, which is in accordance with a previous communication (24) and at variance with other findings (16). The end of the type II CCoV sequence was found at nt 25641, 20 nt downstream of the start codon of the E gene (Fig. 2A). Recombination may have occurred at the donor site between nt 13339 and 13343 and at the acceptor site between nt 25631 and 25641 (Fig. 2B).

At the RNA level, the ORF3abc region showed 92% identity to the genome of the CCoV reference strain Elmo/02. At the protein level the similarity was even higher, 93 and 95% in the case of the 3a and 3c proteins, respectively. However, there is a very significant difference between the ORF3abc regions of FIPV-DF-2 and CCoV Elmo/02. ORF3abc of FIPV DF-2 contained a 338-nt deletion, resulting in a truncated ORF3a and ORF3c and in the complete loss of ORF3b. The original start codon of ORF3a was mutated to ATT, hence it starts from the next in-frame start codon, shortening ORF3a (nt 24867 to 24965) to only 99 nt. Furthermore, due to the deletion mentioned above, the last 12 nt of ORF3a overlap ORF3c. The ORF3c gene (nt 25138 to 25635) was truncated to 498 nt by starting from an alternate in-frame ATG, missing 21 nucleotides from its 3′ end (Fig. 3), and it lacked its own transcription regulatory sequence (TRS) core sequence. The deleted region in the intact CCoV Elmo/02 ORF3abc contained two TRS core sequences (CUAAAC), each one potentially being for the transcription of sg mRNAs 3b and 3c. Regarding the other

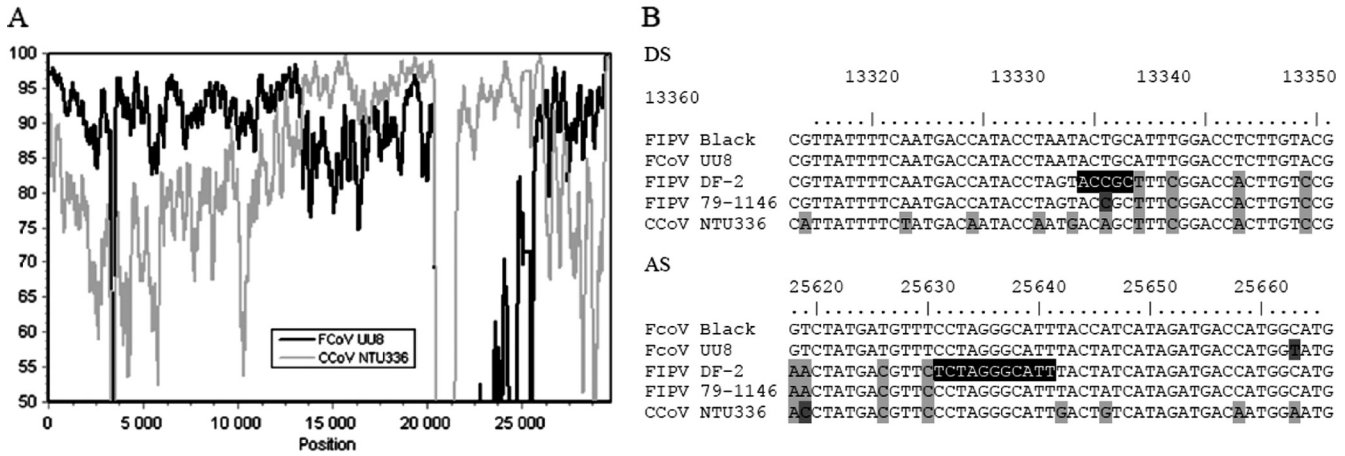

FIG 2 Recombination map of FIPV DF-2. (A) SimPlot analysis of the FIPV DF-2 genome. FIPV DF-2 was compared to the reference strains FCoV UU8 and CCoV NTU336. Percent identity is represented on the *y* axis, and nucleotide positions are shown on the *x* axis. The sliding window was selected as 200 nt, with a step size of 20 nt. (B) Sequence alignment flanking the putative recombination sites of FIPV DF-2. FCoV UU8 and FCoV Black are type I FCoVs, and FIPV DF-2 and FIPV WSU 79-1146 are type II FCoVs. NTU 336 is a CCoV strain. Only sequences flanking the putative donor (DS) and acceptor (AS) recombination sites of FIPV DF-2 are shown. Nucleotides different from the consensus type I sequence are shaded by different tones of gray. Regions where the recombination most probably could have taken place are shaded black.

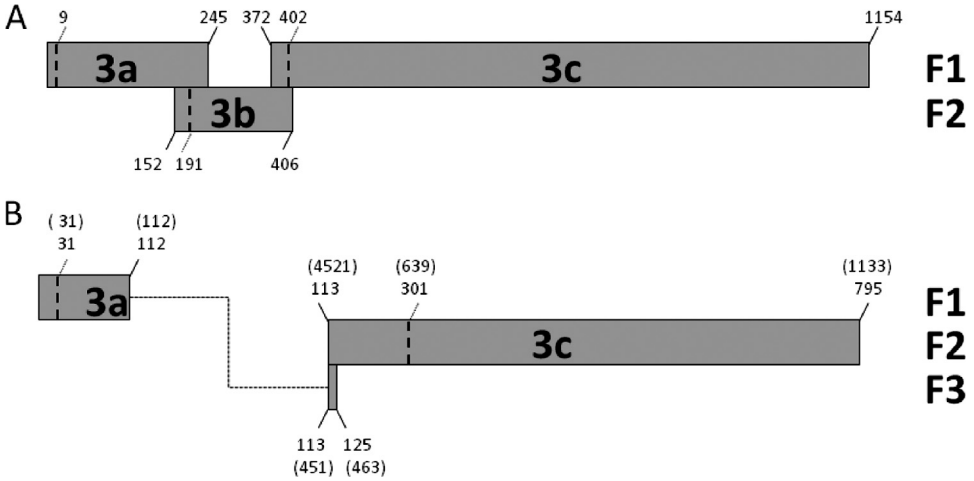

FIG 3 Schematic representation of region 3 of the CCoV Elmo/02 (A) and FIPV DF-2 (B) strains. F1 to F3 represent the three reading frames of the viral genomes. Numbering starts at the first nucleotide of the regions' first core sequence (CUAAAC). The ORFs of interest are symbolized by shaded boxes and are labeled by the number of nucleotides at the beginning and the end. Dashed lines symbolize the first start codon in the ORFs. The dashed connector line represents the deleted part in the DF-2 genome. Numbers in brackets correspond to the numbering of the appropriate nucleotides in region 3 of CCoV Elmo/02.

accessory proteins, which are implicated in the FECV/FIPV transition, ORF7a (nt 27820 to 28125) and ORF7b (nt 28130 to 28750) were intact.

Comparison of the genomic sequence of highly virulent FIPV DF-2 to that of a DF-2 vaccine derivative strain (GenBank accession no. DQ286389) showed the most marked differences, a frameshift and a 2-amino-acid (aa)-long deletion between positions 3317 and 3331, occurred in the nsp6 protein of the vaccine strain. According to various topology prediction programs (25, 48), these mutations affect the primary structure of predicted transmembrane domain 4 of nsp6 (Fig. 4). However, the secondary structure and topological features of nsp6 of the DF-2-derived vaccine strain were not changed, hence the affected region most likely remains a functional part of the transmembrane domain of nsp6 in both strains. More explicit differences were found in the ORF3c protein of the vaccine strain that was 50 aa shorter at the N terminal as a result of a frameshift, and it contained 3 aa substitutions. Furthermore, due to a 406-nt deletion in ORF7b, the gp7b protein of the vaccine strain terminated after the 45th aa, and as a result of a frameshift only the first 40 aa were identical to those of FIPV DF-2. In contrast, the intact 206-aa-long protein was present in the parent virus.

Strategy for cloning of the cDNA encoding infectious FIPV DF-2 RNA. Although reverse genetic systems were previously developed for FCoVs (19, 46), to assemble and express the full-length FIPV DF-2 genome, the pBeloBAC 11 low-copy-number vector was applied as a backbone because of the high stability of exogenous sequences, the relatively easy manipulation of large DNA constructs, and the efficient intracellular production of viral RNA from the cDNA by the CMV immediate-early promoter within transfected cells. Previously, this system was successfully used to rescue transmissible gastroenteritis virus (TGEV) (3), human coronavirus OC43 (43), and severe acute respiratory syndrome coronavirus (SARS-CoV) (5).

Based on the data of the full-length genomic sequence of FIPV DF-2, primers were designed to amplify large overlapping fragments of the whole genome (Table 1). Using unique restriction sites in the overlapping regions, the full-length genome was assembled through eight intermediate constructs (Fig. 1). At the 3′ end, the cDNA was flanked by a 24-bp poly(A) tail followed by the HDV ribozyme to release the full-length genome from the transcribed RNA with a correct 3′ end.

The sequencing of the pBFIPV-DF-2 full-length clone revealed a 1-nt change at position 24429 (G/A) that resulted in an amino acid change in the S protein position 1332 (V/I) and a 1-nt silent mutation at position 26064 (T/C) in the M gene.

The infectious cDNA clone was fully stable during its propagation in *E. coli* DH10B cells through several passages as indicated by EcoRI digestion (data not shown).

Rescue of infectious FIPV from cDNA in FCWF-4 and CrFK cells. To recover infectious FIPV from the full-length cDNA, FCWF-4 cells were transfected with plasmid pBFIPV-DF-2. The

```
TMpred          oooooooooHHHHHHHHHHHHHHHHHHiiiiiiHHHHHHHHHHHHHHH
HMMTOP          oooooooooHHHHHHHHHHHHHHHHHHiiiiiiiiHHHHHHHHHHHHH
DF-2       3301 NVNTTFLPVDMQGVMLALFCVVVFVICTIRFFTCKQSWFSLFATTIFVMF 3350

DF-2 vacc  3301 NVNTTFLPVDMQGVMLHWSVCVLYM--HYKIFTCKQSWFSLFATTIFVMF 3348
HMMTOP          oooHHHHHHHHHHHHHHHHHHHHH--iiiiiiiiiiHHHHHHHHHHHHH
TMpred          ooooooooHHHHHHHHHHHHHHHHHH--HHiiiiiiiiHHHHHHHHHHHHH
```

FIG 4 Alignment and topology prediction of the most divergent part of the nsp6 proteins of the DF-2 and DF-2 vaccine strains. Topology predictions were executed by the TMpred and HMMTOP programs on the full nsp6 proteins; however, only the sites of interest are shown (I, inside loop; o, outside loop; H, transmembrane helix). Numbers indicate the positions of the amino acids in the 1a polyproteins.

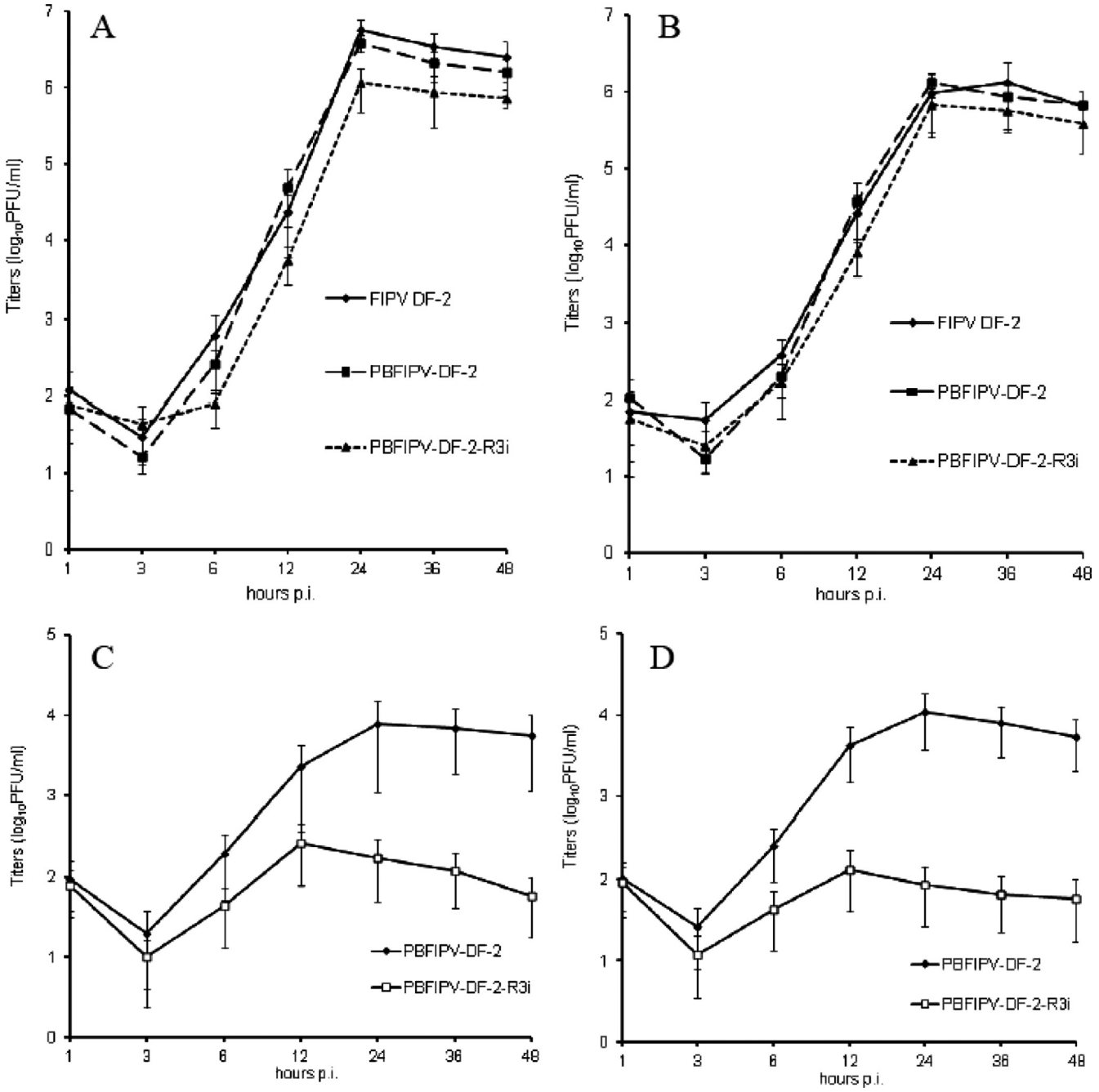

FIG 5 Replication dynamics of the different FCoVs. Growth kinetics of the PBFIPV-DF-2 and PBFIPV-DF-2-R3i recombinant viruses and the parent FIPV DF-2 strain after infection of FCWF-4 (A) and CrFK (B) cells (MOI of 0.1). The titers are given as the means from triplicate experiments (log_{10} $TCID_{50}$/ml); error bars represent standard deviations. Also shown are the growth kinetics of intracellular (C) and extracellular (D) recombinant viruses PBFIPV-DF-2 and PBFIPV-DF-2-R3i after the infection of feline monocytes originating from five different cats (MOI = 5).

CPE produced by the wild-type virus, i.e., the induction of cell fusion and formation of multiple plaques, was observed 12 h post-transfection (p.t.) and became well pronounced by 24 h p.t. In all of the previously described coronaviral BAC systems, a two-step virus recovery process was followed in which 6 h after the transfection of baby hamster kidney-21 (BHK-21) cells, the supernatant was transferred on susceptible cells (4). In contrast, the direct transfection of FCWF-4 with plasmid pBFIPV-DF-2 resulted in excellent virus recovery. The presence of the recombinant virus PBFIPV-DF-2 was confirmed by RT-PCR targeting the characteristic mutations. The supernatant was passaged, and virus titers were compared to those of the wild-type virus. The recombinant virus showed growth characteristics similar to and reached the same 4×10^6-PFU/ml titer as its wild-type counterpart at 24 h p.i. (Fig. 5A). Similar results were obtained using the CrFK cell line (Fig. 5B).

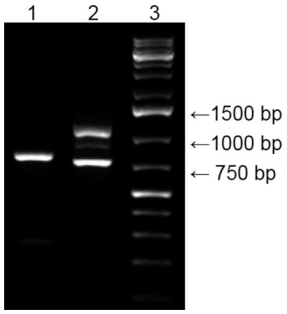

FIG 6 RT-PCR detection of sg mRNA transcription of ORF3abc of PBFIPV-DF-2 and PBFIPV-DF-2-R3i 24 h after infection of CrFK cells (MOI of 0.1). The DF2F forward primer was designed to hybridize to the leader sequence of the FIPV DF-2 genome, while the ORF3CR reverse primer annealed to a sequence stretch of ORF3c present in both viruses. Lane 1, amplification of the ORF3abc sg RNA of PBFIPV-DF-2 resulting in a 804-bp-long amplicon corresponding to the truncated ORF3abc sg mRNA. Lane 2, amplification of the ORF3abc sg RNAs of PBFIPV-DF-2-R3i resulting in three amplicons: a 1,142-bp-long product corresponding to the intact ORF3abc sg mRNA, a 950-bp amplicon corresponding to the ORF3bc sg mRNA, and a 758-bp fragment corresponding to ORF3c sg mRNA. Lane 3, GeneRuler 1-kb Plus DNA ladder (Fermentas).

Construction and rescue of a recombinant FIPV DF-2 with an intact ORF3abc region. The availability of the pBFIPV-DF-2 infectious clone opened the door to investigating the role of the ORF3abc region in the altered cell tropism of FIPV by replacing the truncated ORF3abc with an intact ORF3abc of CCoV origin. The original CCoV that recombined with the ancestor type I FCoV in the ORF3abc region to generate the predecessor of FIPV DF-2 is not known. As a consequence, we decided to choose the genetically closed intact ORF3abc of CCoV Elmo/02 to complement the truncated ORF3abc region of FIPV-DF-2 cDNA. The final pBFIPV-DF-2-R3i recombinant construct contained the complete ORF3abc region from CCoV Elmo/02 but no other undesired mutations, as was confirmed by the full-genome sequencing of the BAC. The recombinant PBFIPV-DF-2-R3i virus rescued after the transfection of FCWF-4 cells revealed somewhat slower growth characteristics compared to those of the parent virus, 1.2×10^6 versus 4×10^6 PFU/ml at 36 h p.i. (Fig. 5A), while in CrFK cells the ORF3abc-complemented virus grew to titers similar to those of the ORF3abc-truncated PBFIPV-DF-2 (Fig. 5B).

Transcription of ORF3abc sg mRNAs. The intactness and stability of the ORF3abc region in the PBFIPV-DF-2-R3i genomic RNA was verified by RT-PCR and sequencing after the third passage. In addition, RT-PCR was applied to investigate the transcription pattern of sg mRNAs in the ORF3abc region on the total RNA extracted from PBFIPV-DF-2- and PBFIPV-DF-2-R3i-infected CrFK cells. The results revealed that the two potential TRS core sequences inside ORF3abc of CCoV Elmo/02, as well as the TRS core sequence preceding this region, served as junction sites for the 5′ viral leader sequence, which was predicted by genome analysis (Fig. 6). This finding strongly suggests that in contrast to the truncated ORF3abc of FIPV DF-2, where only one truncated, shortened mRNA is transcribed, all of the 3a, 3b, and 3c genes are transcribed in PBFIPV-DF-2-R3i-infected cells.

Titration of the recombinant FIPVs in blood monocytes. To investigate the replication kinetics of the ORF3abc truncated/intact recombinant FCoVs in the primary target cells, feline blood monocytes were infected with PBFIPV-DF-2 and PBFIPV-DF-2-R3i. Titers of the extracellular and intracellular viruses were determined by the titration of cell culture supernatant, and cells were collected at different time points on CrFK cells. The results showed that recombinant PBFIPV-DF-2 replication was detectable at 6 h p.i., increased rapidly by 12 h p.i., and then slowed down and peaked at a 0.4×10^4- to 2×10^4-PFU/ml intracellular titer at 24 h p.i. In contrast, the replication of recombinant pBFIPV-DF-2-R3i was detectable at 6 h p.i but peaked at approximately 2 $\log_{10}$ lower values, 3×10^1 to 5×10^2 PFU/ml at 12 h p.i., and then the virus titer significantly decreased (Fig. 5C), indicating a drastically reduced productive infection. The extracellular virus titers showed similar patterns with slightly lower titers (Fig. 5D).

Quantification of genomic and replicative RNA of the recombinant FIPVs. Results of the genomic and subgenomic TaqMan assays, applied to RNA extracted 24 h p.i. from cell lysates of the infected FCWF-4 and CrFK cells as well as from intact feline monocytes, are summarized in Fig. 7. In FCWF-4 cells, pBFIPV-DF-2 reached 1.7×10^8 to 2.1×10^8/ml genomic copy numbers, while only 1.1×10^7 to 1.6×10^7/ml copy numbers were found in the case of pBFIPV-DF-2-R3i, indicating a copy number difference of about one order of magnitude in favor of the recombinant virus containing truncated ORF3abc (Fig. 7A). In CrFK, the genomic copy numbers ranged from 7×10^7 to 1.2×10^8/ml in the case of both pBFIPV-DF-2 and pBFIPV-DF-2-R3i (Fig. 7A). In feline monocytes, pBFIPV-DF-2 reached 2.1×10^5 to 1.2×10^6/ml cellular copy numbers, while pBFIPV-DF-2-R3i gave only 5.3×10^3 to 2.5×10^4/ml, indicating a copy number difference of about two orders of magnitude in favor of the truncated ORF3abc-containing virus (Fig. 7B). Data from the TaqMan assay targeting the replicative RNA of the recombinant viruses gave similar results and confirmed the presence of virus replication (Fig. 7B).

DISCUSSION

The analysis of the full-length genome sequence of FIPV DF-2 revealed 99% nucleotide identity to FIPV WSU-79/1146 and, based on the available partial sequence, to strain Nor15, suggesting that the three viruses share a recent common ancestor. The comparison of the sequences of FIPV DF-2 and a DF-2 vaccine derivate strain (DQ286389) revealed a striking difference in the nsp6 coding region. The 2-aa deletion and frameshift affected the transmembrane domain 4 region, but based on topology predictions, the anchor function of this domain (6) might have remained intact. However, these mutations might influence the interactions of nsp6, and this deletion alone or in combination with other point mutations in the polymerase complex might be responsible for the thermosensitivity of the vaccine virus. The ORF7b gene of FIPV DF-2 was found to be intact, while it was shortened to 20% of its original length in the vaccine virus. The large deletions characteristic of the ORF7b gene FIPV strains subjected to serial tissue culture passages led to increased fitness *in vitro* but caused the loss of virulence *in vivo* (20, 36), which could explain the attenuated phenotype of the vaccine.

Even though several publications imply the involvement of ORF3abc in the pathogenesis of FIP, very little is known about the exact functions of the proteins encoded by this genetic region (21, 36). The presence of ORF3a and ORF3b is a distinctive feature for FCoV, CCoV, and transmissible gastroenteritis virus (TGEV) of the alphacoronavirus genus. The genome of these viruses encodes

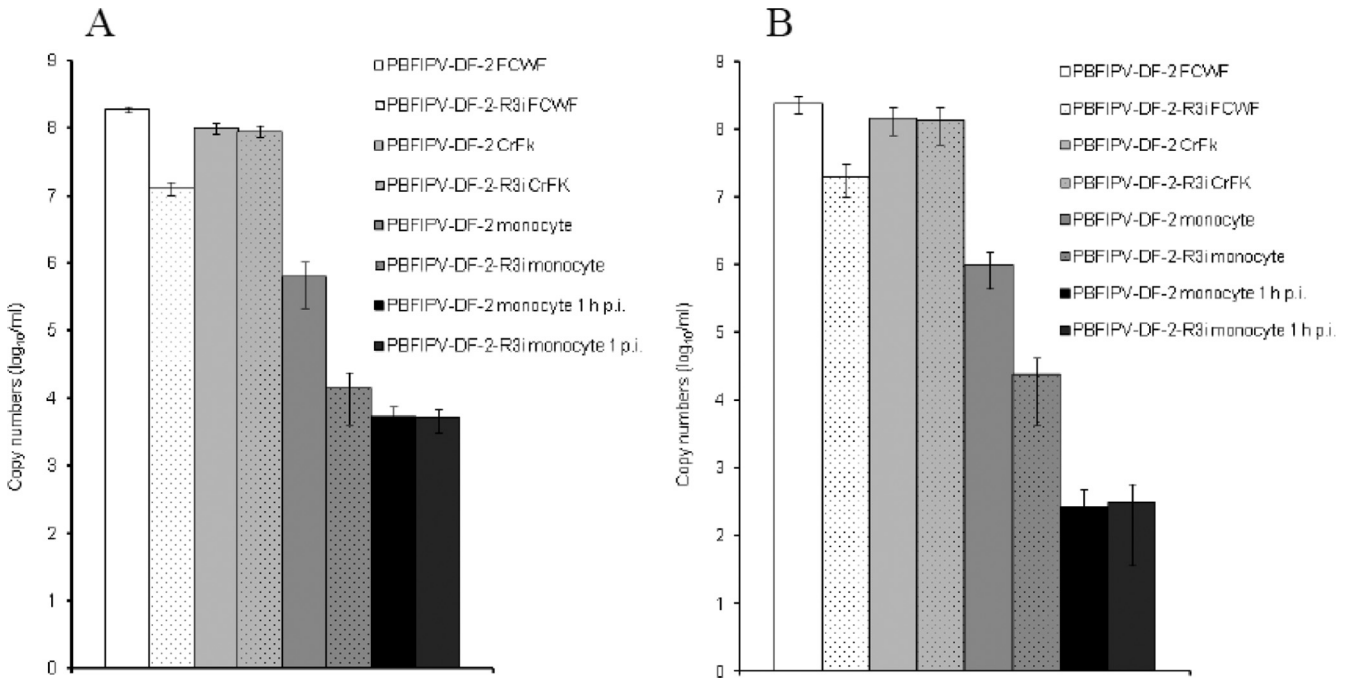

FIG 7 Quantification of genomic and replicative RNA. Copy numbers of FIPV DF2 and recombinant viruses PBFIPV-DF-2 and PBFIPV-DF-2-R3i at 24 h p.i. in FCWF-4 cells, CrFK cells (MOI = 0.1), and feline monocytes originating from five different cats (MOI of 5) with genomic (A) and subgenomic (B) TaqMan assays.

two proteins of approximately 80 and 70 aa, respectively, with unknown function. However, it is known that a deletion truncating CCoV ORF3b contributes to the change of cell tropism and to the development of the systemic infection of pups (11). ORF3c (coronavirus NS3b superfamily; Pfam no. PF03053) is a membrane protein and a characteristic feature of the alphacoronaviruses. Despite the lack of sequence homology, it shows a hydrophobicity profile that is remarkably similar to that of coronaviral M proteins and 3a protein of SARS-CoV (38). Although the majority of functional motifs (cysteine-rich domain, diacidic domain, and RNA binding C-terminal domain) identified in SARS-CoV 3a (8) cannot be found on FCoV 3c, the presence of three transmembrane domains and the genome localization suggest similar regulating functions of FCoV 3c and SARSV-CoV 3a proteins (35). The SARS-CoV 3a structural protein alters the intracellular trafficking of S, resulting in a decrease of its surface expression (45). It induces cell death, Golgi fragmentation, the accumulation of intracellular vesicles (18), and cell apoptosis (47). In addition, it is a potassium channel protein that has been involved in virus release (8, 32), and it plays a role in attenuating interferon responses and innate immunity (34).

Several researchers investigated the growth kinetics of different FIPV and FECV strains (14, 33, 41, 44). These studies revealed that while the replication characteristics of FIPV and FECV are rather similar in continuous cell lines such as CrFK (14, 33) and FCWF-4 (41), in the natural target cells of FIPV, the feline primary macrophage/monocyte cells, FECVs were less able to sustain viral replication and produced approximately 2 $\log_{10}$ lower virus titers in peritoneal macrophages (44), feline blood monocytes (14), and primary bone marrow-derived macrophages (41). However, these experiments have not elucidated the role of ORF3abc in the altered tropism of the FIPV/FECV virus pair, because genetic differences affected several other regions of the virus genome as well.

To obtain a definite answer about the role of ORF3abc in altered macrophage/monocyte tropism, our approach was to generate a genetically identical FCoV pair, differing only in their ORF3abc region. Using the BAC-based reverse genetics system, the truncated ORF3abc of FIPV DF-2 was replaced with an intact, genetically closely related ORF3abc region from the CCoV Elmo/02 (39). In the recombinant strain PBFIPV-DF-2-R3i, ORF3a, ORF3b, and ORF3c are preceded by canonical TRSs, suggesting their independent transcription as shown by RT-PCR. The *in vitro* growth kinetics of the ORF3abc truncated/intact virus pair PBFIPV-DF-2 and PBFIPV-DF-2-R3i was compared in cell lines and feline peripheral blood monocytes. The CrFK cell line with epithelial origin was shown earlier to be equally permissive for both FIPV and FECV strains (14, 33), so it is not surprising that two recombinant viruses, PBFIPV-DF-2 and PBFIPV-DF-2-R3i, reached the same titers in this cell line. However, a marked difference was found in blood monocytes, where PBFIPV-DF-2 replication revealed about 2 to 2.5 $\log_{10}$ higher virus titers than those of PBFIPV-DF-2-R3i. The quantitative RT-PCR analysis of the genomic and replicative RNA form confirmed these findings.

Previous *in vitro* studies showed that FIPV replicated in feline macrophages/monocytes more efficiently than FECV (14, 41, 44). While the contribution of proteins other than 3abc in the altered tissue tropism cannot be excluded due to the different genetic backgrounds of these FCoV strains, our results unambiguously show that the presence of intact 3abc inhibits the productive FCoV infection of feline monocytes. The slight, 0.5 $\log_{10}$ replication difference between the ORF3abc truncated and intact recombinant viruses in FCWF-4 cells might also be explained by some macrophage characteristics of these cell line (nonspecific esterase, phagocytic activity, and Fc receptors) (28); however, the viral replication kinetics in FCWF-4 significantly differs from that of primary macrophages/monocytes.

In conclusion, our *ex vivo* infection experiments with an FIPV strain and a repaired ORF3abc that was otherwise genetically identical to FCoV seem to confirm the hypothesis that the truncated ORF3abc plays an important role in the acquisition of macrophage/monocyte tropism of type II FIPV, and they suggest that the alteration of this region is an important factor in the development of FIP pathogenesis.

ACKNOWLEDGMENTS

This work was supported by the Award of Excellence from the Swedish University of Agricultural Sciences, research grants from the AGRIA Animal Insurance Company (Agria Djurförsäkring), OTKA, and NKTH (Mobilitás 08-C OTKA 81187), the János Bolyai Fellowship from the Hungarian Academy of Sciences (BO/00414/10), and the Ministry of Science and Innovation of Spain (MCINN) (BIO2010-16705).

REFERENCES

1. **Addie D, Jarrett O.** 1992. A study of naturally occurring feline coronavirus infections in kittens. Vet. Rec. **130**:133–137.
2. **Addie D, et al.** 2009. Feline infectious peritonitis. ABCD guidelines on prevention and management. J. Feline Med. Surg. **11**:594–604.
3. **Almazan F, et al.** 2000. Engineering the largest RNA virus genome as an infectious bacterial artificial chromosome. Proc. Natl. Acad. Sci. U. S. A. **97**:5516–5521.
4. **Almazan F, Galan C, Enjuanes L.** 2004. The nucleoprotein is required for efficient coronavirus genome replication. J. Virol. **78**:12683–12688.
5. **Almazan F, et al.** 2006. Construction of a severe acute respiratory syndrome coronavirus infectious cDNA clone and a replicon to study coronavirus RNA synthesis. J. Virol. **80**:10900–10906.
6. **Baliji S, Cammer SA, Sobral B, Baker SC.** 2009. Detection of nonstructural protein 6 in murine coronavirus-infected cells and analysis of the transmembrane topology by using bioinformatics and molecular approaches. J. Virol. **83**:6957–6962.
7. **Biek R, et al.** 2006. Factors associated with pathogen seroprevalence and infection in Rocky Mountain cougars. J. Wildl. Dis. **42**:606–615.
8. **Chan CM, et al.** 2009. The ion channel activity of the SARS-coronavirus 3a protein is linked to its pro-apoptotic function. Int. J. Biochem. Cell Biol. **41**:2232–2239.
9. **Chang HW, de Groot RJ, Egberink HF, Rottier PJ.** 2010. Feline infectious peritonitis; insights into feline coronavirus pathobiogenesis and epidemiology based on genetic analysis of the viral 3c gene. J. Gen. Virol. **91**:415–420.
10. **Chang HW, Egberink HF, Rottier PJ.** 2011. Sequence analysis of feline coronaviruses and the circulating virulent/avirulent theory. Emerg. Infect. Dis. **17**:744–746.
11. **Decaro N, et al.** 2007. Molecular characterisation of the virulent canine coronavirus CB/05 strain. Virus Res. **125**:54–60.
12. **Decaro N, Buonavoglia C.** 2008. An update on canine coronaviruses: viral evolution and pathobiology. Vet. Microbiol. **132**:221–234.
13. **de Groot-Mijnes JD, van Dun JM, van der Most RG, de Groot RJ.** 2005. Natural history of a recurrent feline coronavirus infection and the role of cellular immunity in survival and disease. J. Virol. **79**:1036–1044.
14. **Dewerchin HL, Cornelissen E, Nauwynck HJ.** 2005. Replication of feline coronaviruses in peripheral blood monocytes. Arch. Virol. **150**:2483–2500.
15. **Dye C, Siddell SG.** 2005. Genomic RNA sequence of feline coronavirus strain FIPV WSU-79/1146. J. Gen. Virol. **86**:2249–2253.
16. **Dye C, Siddell SG.** 2007. Genomic RNA sequence of feline coronavirus strain FCoV C1Je. J. Feline Med. Surg. **9**:202–213.
17. **Evermann JF, Baumgartener L, Ott RL, Davis EV, McKeirnan AJ.** 1981. Characterization of a feline infectious peritonitis virus isolate. Vet. Pathol. **18**:256–265.
18. **Freundt EC, et al.** 2010. The open reading frame 3a protein of severe acute respiratory syndrome-associated coronavirus promotes membrane rearrangement and cell death. J. Virol. **84**:1097–1109.
19. **Haijema BJ, Volders H, Rottier PJ.** 2003. Switching species tropism: an effective way to manipulate the feline coronavirus genome. J. Virol. **77**:4528–4538.
20. **Haijema BJ, Volders H, Rottier PJ.** 2004. Live, attenuated coronavirus vaccines through the directed deletion of group-specific genes provide protection against feline infectious peritonitis. J. Virol. **78**:3863–3871.
21. **Haijema BJ, Rottier PJ, de Groot JR.** 2007. Feline coronaviruses: a tale of two-faced types, p 183–203. *In* V. Thiel (ed), Coronaviruses: molecular and cellular biology. Caister Academic Press, Norfolk, United Kingdom.
22. **Heeney JL, et al.** 1990. Prevalence and implications of feline coronavirus infections of captive and free-ranging cheetahs (Acinonyx jubatus). J. Virol. **64**:1964–1972.
23. **Herrewegh AA, Vennema H, Horzinek MC, Rottier PJ, de Groot RJ.** 1995. The molecular genetics of feline coronaviruses: comparative sequence analysis of the ORF7a/7b transcription unit of different biotypes. Virology **212**:622–631.
24. **Herrewegh AA, Smeenk I, Horzinek MC, Rottier PJ, de Groot RJ.** 1998. Feline coronavirus type II strains 79-1683 and 79-1146 originate from a double recombination between feline coronavirus type I and canine coronavirus. J. Virol. **72**:4508–4514.
25. **Hofmann K, Stoffel W.** 1993. TMBASE–a database of membrane spanning protein segments. Biol. Chem. Hoppe-Seyler **374**:166.
26. **Hofmann-Lehmann R, et al.** 1996. Prevalence of antibodies to feline parvovirus, calicivirus, herpesvirus, coronavirus, and immunodeficiency virus and of feline leukemia virus antigen and the interrelationship of these viral infections in free-ranging lions in east Africa. Clin. Diagn. Lab. Immunol. **3**:554–562.
27. **Hohdatsu T, Okada S, Ishizuka Y, Yamada H, Koyama H.** 1992. The prevalence of types I and II feline coronavirus infections in cats. J. Vet. Med. Sci. **54**:557–562.
28. **Jacobse-Geels HE, Horzinek MC.** 1983. Expression of feline infectious peritonitis coronavirus antigens on the surface of feline macrophage-like cells. J. Gen. Virol. **64**:1859–2866.
29. **Kennedy M, Boedeker N, Gibbs P, Kania S.** 2001. Deletions in the 7a ORF of feline coronavirus associated with an epidemic of feline infectious peritonitis. Vet. Microbiol. **81**:227–234.
30. **Kummrow M, et al.** 2005. Feline coronavirus serotypes 1 and 2: seroprevalence and association with disease in Switzerland. Clin. Diagn. Lab. Immunol. **12**:1209–1215.
31. **Lole KS, et al.** 1999. Full-length human immunodeficiency virus type 1 genomes from subtype C-infected seroconverters in India, with evidence of intersubtype recombination. J. Virol. **73**:152–160.
32. **Lu W, et al.** 2006. Severe acute respiratory syndrome-associated coronavirus 3a protein forms an ion channel and modulates virus release. Proc. Natl. Acad. Sci. U. S. A. **103**:12540–12545.
33. **McKeirnan AJ, Evermann JF, Davis EV, Ott RL.** 1987. Comparative properties of feline coronaviruses *in vitro.* Can. J. Vet. Res. **51**:212–216.
34. **Minakshi R, et al.** 2009. The SARS coronavirus 3a protein causes endoplasmic reticulum stress and induces ligand-independent downregulation of the type 1 interferon receptor. PLoS One **4**:e8342.
35. **Oostra M, de Haan CA, de Groot RJ, Rottier PJ.** 2006. Glycosylation of the severe acute respiratory syndrome coronavirus triple-spanning membrane proteins 3a and M. J. Virol. **80**:2326–2336.
36. **Pedersen NC.** 2009. A review of feline infectious peritonitis virus infection: 1963–2008. J. Feline Med. Surg. **11**:225–258.
37. **Pedersen NC, Liu H, Dodd KA, Pesavento PA.** 2009. Significance of coronavirus mutants in feces and diseased tissues of cats suffering from feline infectious peritonitis. Viruses **1**:166–184.
38. **Pedersen NC, et al.** 17 January 2012. Feline infectious peritonitis: role of the feline coronavirus 3c gene in intestinal tropism and pathogenicity based upon isolates from resident and adopted shelter cats. Virus Res. [Epub ahead of print] doi:10.1016/j.virusres.2011.12.020.
39. **Pratelli A, et al.** 2003. Genetic diversity of a canine coronavirus detected in pups with diarrhoea in Italy. J. Virol. Methods **110**:9–17.
40. **Reed LJ, Muench H.** 1938. A simple method of estimating fifty percent endpoints. Am. J. Hyg. **27**:493–497.
41. **Rottier PJ, Nakamura K, Schellen P, Volders H, Haijema BJ.** 2005. Acquisition of macrophage tropism during the pathogenesis of feline infectious peritonitis is determined by mutations in the feline coronavirus spike protein. J. Virol. **79**:14122–14130.
42. **Sambrook J, Fritsch EF, Maniatis T.** 2001. Molecular cloning: a laboratory manual, 3rd ed. Cold Spring Harbor Laboratory Press, Cold Spring Harbor, NY.
43. **St.-Jean JR, et al.** 2006. Recovery of a neurovirulent human coronavirus OC43 from an infectious cDNA clone. J. Virol. **80**:3670–3674.
44. **Stoddart CA, Scott FW.** 1989. Intrinsic resistance of feline peritoneal macrophages to coronavirus infection correlates with in vivo virulence. J. Virol. **63**:436–440.

45. **Tan YJ.** 2005. The severe acute respiratory syndrome (SARS)-coronavirus 3a protein may function as a modulator of the trafficking properties of the spike protein. Virol. J. **2**:5.
46. **Tekes G, Hofmann-Lehmann R, Stallkamp I, Thiel V, Thiel HJ.** 2008. Genome organization and reverse genetic analysis of a type I feline coronavirus. J. Virol. **82**:1851–1859.
47. **Tsui SK.** 2009. Functional roles of 3a protein in the pathogenesis of SARS. Hong Kong Med. J. Suppl. **8**:19–20.
48. **Tusnády GE, Simon I.** 2001. The HMMTOP transmembrane topology prediction server. Bioinformatics **17**:849–850.
49. **Vennema H, Poland A, Foley J, Pedersen NC.** 1998. Feline infectious peritonitis viruses arise by mutation from endemic feline enteric coronaviruses. Virology **243**:150–157.
50. **Wang K, Boysen C, Shizuya H, Simon MI, Hood L.** 1997. Complete nucleotide sequence of two generations of a bacterial artificial chromosome cloning vector. Biotechniques **23**:992–994.